Supporting Information

Electrochemical CO_2 Reduction to Methanol by Cobalt Phthalocyanine: Quantifying CO_2 and CO Binding Strengths and Their Influence on Methanol Production

Libo Yao[a,b,#], *Kevin E. Rivera-Cruz*[b,#], *Paul M. Zimmerman*[*,b], *Nirala Singh*[*,a], *Charles C. L. McCrory*[*,b,c]

[a] Department of Chemical Engineering, University of Michigan, Ann Arbor, MI, 48109, United States

[b] Department of Chemistry, University of Michigan, Ann Arbor, MI, 48109, United States

[c] Macromolecular Science & Engineering Program, University of Michigan, Ann Arbor, MI, 48109, United States

[*]Corresponding Authors:

Charles C. L. McCrory cmccrory@umich.edu

Nirala Singh snirala@umich.edu

Paul M. Zimmerman paulzim@umich.edu

Contents

Supplementary Section 1: Experimental Methods

1.1 Materials

Carbon dioxide (CO_2, 99.999%), carbon monoxide (CO, 99.9%), and nitrogen (N_2, 99.9%) were purchased from Cryogenic Gases. $^{13}CO_2$ (99.8%, CLM-185-1-LB) and ^{13}CO (99.0%, CLM-189-1LB) were purchased from Cambridge Isotope Laboratory. Cobalt phthalocyanine (CoPc, 97%), multi-walled carbon nanotube (MWCNT, > 98% carbon basis), Nafion^{TM} 117 containing solutions (~5 wt%), nitric acid (HNO_3, TraceMetal grade, 67-70%), *N*, *N*-Dimethylformamide (DMF, ACS grade) were purchased from Sigma Aldrich. Potassium bicarbonate ($KHCO_3$, certified ACS) was purchased from Fisher Scientific. Freudenberg H23C6 carbon paper and Nafion^{TM} 117 proton exchange membrane were purchased from Fuel Cell Store. IrO_2 gas diffusion electrode was purchased from Dioxide Materials.

1.2 Preparation of CoPc/CNT catalysts

Before the preparation, pretreatment of carbon nanotubes was performed based on the reported method to remove possible metal impurities. The preparation method was detailed in our previous work.[1] In general, CoPc was dissolved in DMF solution to form a 0.2 mM CoPc/DMF solution, then a given weight of CNT was added to the solution and sonicated for 30 min. The suspension was then stirred at least 12 h to ensure complete dispersion, followed by centrifugation at 7000 rpm for 45 min under −11 ℃. After decanting the DMF solution, the remaining pellet was washed and filtrated with DMF solvent until the filtrated liquid turned colorless. The CoPc/CNT sample was then dried at under 80 ℃ for 2 hr and then stored in a vacuum desiccator overnight.

1.3 Determination of cobalt loading

The loading of cobalt onto the electrodes was determined using inductively coupled plasma mass spectrometry (ICP-MS). 15 mL 1 M TraceMetal HNO_3 solution was added to the given mass of the CoPc/CNT sample, the resulting mixture was stirred under 900 rpm overnight. The slurry was then filtered using a cellulose syringe (0.45 μm, Titan 3 regenerated cellulose, Fisher Scientific) to remove the CNT. The filtered solution was analyzed in ICP-MS using the Co calibration standards in 1 M HNO_3 at 0, 10, 50, 100, and 500 ppb.

1.4 Electrochemical measurement

Most electrochemical measurements were conducted in a homemade CO_2 reduction flow electrolyzer using a 3-electrode system, as shown in Figure S1. Supplementary experiments for batch CO_2RR and CORR were conducted in a sealed, aqueous H-cell reactor. The reaction setup and experimental methods are detailed in our previous publication.[1] For the preparation of catalyst deposition ink, CoPc/CNT and Nafion^{TM} 117 solution were added to a 2-propanol solution with a 2:1 mass ratio. The ink was sonicated for 30 min and deposited onto Freudenberg H23C6 carbon paper using the airbrushing method, forming a CoPc/CNT (or CoPc(py)/CNT) gas diffusion electrode (GDE). The mass loading for CoPc/CNT was controlled at 0.27 mg/cm^2 (normalized by the geometric area of the carbon paper) on the GDE and the total cobalt loading was determined by ICP-MS described above, and the Co molar loading on the GDE is determined as (9.0 ± 1.1) $*10^{-9}$ mol/cm^2.

The electrochemical measurements were conducted using a Bio-Logic VSP potentiostat. Chronoamperometry (CA) mode was used to perform CO and/or CO_2 reduction under given potentials. For flow cell experiments, the electrolysis was conducted for 10 min. iR correction was applied using the ZIR mode with an 85% compensation rate. CoPc/CNT GDE was used as the working electrode and the IrO_2 electrode purchased from Dioxide Materials was used as the

counter electrode. The cathode and anode chambers were separated by the Nafion^{TM} 212 membrane. A Leakless Ag/AgCl electrode (eDAQ) was used as a reference electrode and inserted in the cathode chamber. 0.5 M $KHCO_3$ with a pH of 8.5 was used as the electrolyte for all experiments. 15 mL/min gas was fed through the gas compartment close to the cathode. The gas stream exiting the gas compartment on the cathode side was connected to GC for product analysis. Both the cathode and anode chambers were flowed with 0.8 mL/min electrolyte using peristaltic pumps. To better quantify the liquid products for single-pass conversion, the electrolyte was not recycled but was directly collected for quantification after it exited the flow cell. For H-cell experiments, the electrolysis was conducted for 1 h to ensure quantifiable products were generated. No iR compensation was applied. Glassy carbon electrodes supporting CoPc/CNT inks were used as working electrode. Saturated calomel electrode (SCE) was used as reference electrode and graphite rod was used as counter electrode. For the electrolysis, the main chamber was filled with 30 mL electrolyte and the volume of the headspace was measured each time after the reaction. Prior to each experiment, both chambers were sparged with CO_2 for ~ 30 min and then the main chamber was sealed in CO_2 atmosphere. After the reaction a gastight reusable syringe was used to extract the gas within the main chamber and injected into gas chromatography (GC) for quantification of gas products. ^{1}H NMR was used for quantification of liquid products.

1.5 Product quantification

Gas effluents were analyzed and quantified in-line via a Shimadzu GC-2030 gas chromatograph equipped with a thermal conductivity detector (TCD) and a flame ionization detector (FID). The two gas products, CO and H_2, were calibrated using calibration gas mixtures (SCOTTY Specialty Gas) at concentration levels of 0.02, 0.05, 0.5, and 1.0% v/v.

For CO and H_2, Faradaic efficiencies (FE) were calculated using eq. S1:

$$FE = \frac{\frac{pV_{out}}{RT} \times C \times 2F}{Q/t} \quad \text{(eq. S1)}$$

Where p is the pressure of the outlet gas flow, R is the ideal gas constant, T is absolute temperature, V_{out} (m^3/s) is the flow rate exiting the flow cell, t (s) is the reaction time, C is the volume percentage of the product determined by GC (%), F is the Faraday constant (96485 C/mol), and Q (C) is the total charge passed during the reaction time.

Liquid products were qualitatively analyzed by ^{1}H-NMR with water suppression method using a Varian MR400 nuclear magnetic resonance (NMR) instrument. 500 µL of the collected liquid sample was mixed with 100 µL of deuterium oxide (D_2O), which contained 1.37 mM dimethyl sulfoxide (DMSO) as external standard. Faradaic efficiency of methanol (FE_{Me}) can be calculated using eq. S2:

$$FE = \frac{C_{Me} \times V_{liq} \times n \times F}{Q} \quad \text{(eq. S2)}$$

Where C_{Me} (mol/L) is the detected concentration for methanol, V_{liq} is the total volume of the collected liquid, n is the number of electrons passed for the formation of 1 methanol molecule. For CO reduction $n = 4$ and CO_2 reduction $n = 6$. Note that in the CO/CO_2 co-feeding experiments, precise quantification of CO is challenging due to the dual role of CO as both a reactant and a product. Therefore, both the j_{CH3OH} and FE_{CH3OH} are quantified based on a four-electron transfer reaction by assuming all the CH_3OH was produced from CO, and $j$co and FE_{CO} are not calculated.

The single pass conversion of CO_2 (X_{CO2}) is calculated based on the based on the formation of CO and CH_3OH, the two products generated via CO_2RR, as shown in eq. S3:

$$X_{CO2} = \frac{n_{CO2} - n_{CO} - n_{CH3OH}}{n_{CO2}} \quad \text{(eq. S3)}$$

Where n_{CO2} (mol/s) represents the molar flow rate of CO_2 entering the flow cell, n_{CO} and n_{CH3OH} represent the molar formation rates of CO and CH_3OH.

Supplementary Section 2: Derivation of Microkinetic Models

The derivation of microkinetic models for CORR and CO_2RR is performed based on experimental *j*−*P* relationship shown in Figure 1. The current densities of CH_3OH (j_{CH3OH}) and CO (j_{CO}) are correlated to the partial pressures of CO (P_{CO}) and CO_2 (P_{CO2}) from the bulk gas feeding for the respective reactions (CORR and CO_2RR). Rate laws were derived based on proposed elementary steps, and numerical fitting was applied to fit the experimental data to determine the most possible model. Based on the fitting results, the equilibrium constants for CO and CO_2 binding (denoted as K_{CO} and K_{CO2}) are obtained. Note that the *j*−*P* relationship illustrates a correlation between partial current density and the bulk concentration of reactant, while it is the local concentration that intrinsically determines the reaction rate. To bridge the gap between the bulk and local properties and also to validify the *P*-dependent derivation, two assumptions are made and stated below:

1) The local CO and CO_2 concentration is a regular function of the measured P_{CO} and P_{CO2};
2) Equilibrium of CO and CO_2 binding is rapidly achieved at any given P_{CO} or P_{CO2}.

We deem both assumptions reasonable. The first assumption is supported by Henry's Law and Fick's Law, by combining them the local concentrations of CO/CO_2 are directly correlated to their respective partial pressures in the bulk gas feed. The second assumption is a common assumption made in microkinetic analysis when binding or adsorption is fast relative to chemical reactions.[2,3]

2.1 Microkinetic analyses for CO reduction to CH_3OH on CoPc catalyst

Based on previous mechanistic studies, the active CoPc species for CO_2/CO binding is the singly reduced intermediate, which is denoted as $[CoPc]^-$.[3–5] Therefore, we consider the one-electron reduction of $[CoPc]$ as the first step of both the COR and CO_2R reaction pathways, followed by the binding of CO/CO_2 and the subsequent protonation steps. Detailed reaction pathways and microkinetic analyses are discussed in the following.

To derive the rate law for CO-to-CH_3OH reaction, we write down the proposed reaction steps for CO reduction to methanol on CoPc catalyst. The reaction steps after $[CHO-CoPc]$ are merged into one equation (Step 4) as they have no significant impact on the rate law:

1. $CoPc + e^- \overset{K_{[CoPc]}}{\longleftrightarrow} [CoPc]^-$
2. $[CoPc]^- + CO \overset{K_{CO}}{\longleftrightarrow} [CO-CoPc]^-$
3. $[CO-CoPc]^- + H_2O \xrightarrow{k_{[CO-CoPc]^-}} [CHO-CoPc] + OH^-$
4. $[CHO-CoPc] \overset{K_{CH3OH}}{\longleftrightarrow} [CH_3OH-CoPc]$

Note that the pristine cobalt phthalocyanine is denoted as $CoPc$, all the other reduced CoPc or bound intermediates are enclosed with square brackets. The overall charges of the intermediates are labeled outside the brackets. The K values are equilibrium constants for given reaction steps, k value represents rate constant for the proposed rate determining step. (RDS)

Assumption 1: Step 3 as the rate-determining step (RDS).

1. $CoPc + e^- \overset{K_{[CoPc]}}{\longleftrightarrow} [CoPc]^-$
2. $[CoPc]^- + CO \overset{K_{CO}}{\longleftrightarrow} [CO - CoPc]^-$
3. $[CO - CoPc]^- + H_2O \xrightarrow{k_{[CO-CoPc]^-}} [CHO - CoPc] + OH^-$ RDS
4. $[CHO - CoPc] \overset{K_{CH3OH}}{\longleftrightarrow} [CH_3OH - CoPc]$

We assume the protonation of $[CO - CoPc]^-$ intermediate, i.e., Step 3, is the RDS. The current density of methanol, j_{CH3OH}, can be represented as:

$$j_{CH3OH} = k_{[CO-CoPc]^-} C([CO - CoPc]^-) \quad \text{(eq. S6)}$$

$C([CO - CoPc]^-)$ represents the concentration of the intermediate $[CO - CoPc]^-$, similar notation will be used throughout the entire section.

Quasi-equilibrium for CO binding is assumed, the equilibrium constant for CO binding, K_{CO}, can be represented as:

$$K_{CO} = \frac{C([CO-CoPc]^-)}{C([CoPc]^-)P_{CO}} \quad \text{(eq. S7)}$$

We assume CO as the main adsorbate, the total active sites $[CoPc]^-_{all}$ can be represented as:

$$C([CoPc]^-_{all}) = C([CoPc]^-) + C([CO - CoPc]^-) \quad \text{(eq. S8)}$$

We combine eq. S7 and eq. S8:

$$C([CO - CoPc]^-) = \frac{K_{CO}P_{CO}}{1+K_{CO}P_{CO}} C([CoPc]^-_{all}) \quad \text{(eq. S9)}$$

Thus, the methanol current density is given by eq. S10 through combining eq. S6 and S9:

$$j_{CH3OH} = k_{[CO-CoPc]^-} \frac{K_{CO}P_{CO}}{1+K_{CO}P_{CO}} C([CoPc]^-_{all}) \quad \text{(eq. S10)}$$

We combine all constant terms into one parameter, k_{CO}

$$k_{CO} = k_{[CO-CoPc]^-} C([CoPc]^-_{all}) \quad \text{(eq. S11)}$$

j_{CH3OH} can then be written as:

$$j_{CH3OH} = k_{CO} \frac{K_{CO}P_{CO}}{1+K_{CO}P_{CO}} \quad \text{(eq. S12)}$$

Assumption 2: Step 2 as the rate-determining step.

1. $CoPc + e^- \overset{K_{[CoPc]}}{\longleftrightarrow} [CoPc]^-$
2. $[CoPc]^- + CO \overset{k'_{CO}}{\longrightarrow} [CO-CoPc]^-$ RDS
3. $[CO-CoPc]^- + H_2O \overset{K_{[CO-CoPc]^-}}{\longleftrightarrow} [CHO-CoPc] + OH^-$
4. $[CHO-CoPc] \overset{K_{CH3OH}}{\longleftrightarrow} [CH_3OH-CoPc]$

The current density of methanol j_{CH3OH} if step 2 is the RDS can be represented as:

$$j_{CH3OH} = k'_{CO} C([CoPc]^-) P_{CO} \quad \text{(eq. S13)}$$

Where k'_{CO} is the rate constant of CO binding. Assume quasi-equilibrium for CoPc reduction (step 1), then:

$$K_{[CoPc]} = \frac{C([CoPc]^-)}{C([CoPc])\exp\left(\frac{\eta F}{RT}\right)} \quad \text{(eq. S14)}$$

Where exp ($\frac{\eta F}{RT}$) is the adapted Nernst equation, F is the Faraday constant, and η is the overpotential. Under a fixed applied potential, this term can be treated as a constant.[6]

$$j_{CH3OH} = k'_{CO} K_{[CoPc]} C([CoPc]) \exp\left[\frac{\eta F}{RT}\right] P_{CO} \quad \text{(eq. S15)}$$

Combine all constant terms into one parameter, k_{CO}, the j_{CH3OH} can be written as:

$$j_{CH3OH} = k_{CO} P_{CO} \quad \text{(eq. S16)}$$

By fitting eq. S12 and eq. S16 to the partial pressure-dependent data shown in Figure 1a using the MATLAB code provided in Supplementary Section 3, eq. S12 has a better fit to the experimental data shown in Figure 1a, while eq. S16 only demonstrates a linear correlation to P_{CO}, which does not match the experimental results. Therefore Step 3, i.e., the protonation of $[CO - CoPc]^-$ is a more likely RDS for COR to methanol, hence the numerical fitting will be conducted using the rate law derived from Assumption 1.

Numerical fitting of j_{CH3OH}-P_{CO} data points

We fitted the experimental j_{CH3OH}-P_{CO} data with eq. S12 using MATLAB and the results are shown in Figure 1a. The fitted values for k_{CO} and K_{CO} are tabulated in Table S1, together with the r-square (R^2), root-mean-square deviation (RMSD), and p-value at 95% confidence interval.

Table S1. Fitted parameters for the j_{CH3OH}-P_{CO} data points.

k_{CO} (mA/cm^2)	K_{CO} (atm^{-1})	R^2	RMSD	p-value (95% confidence interval)	
				k_{CO}	K_{CO}
40.9	3.4	0.9682	1.83	0.000012	0.225

2.2 Microkinetic analyses for CO_2 reduction to CO on CoPc catalyst

A similar process to what's illustrated in Section 2.1 has been used to derive the rate law for CO_2RR. Note that the rate law of CO_2RR was derived from CO_2-to-CO reaction, despite CH_3OH was also generated from the CO_2RR cascade reaction when $P_{CO2} < 0.1$ atm. However, the j_{CH3OH} is low (< 3 mA/cm^2) under any given P_{CO2} so it is reasonable to neglect the CH_3OH formation and derive the rate only from CO production.

The reaction steps for CO_2-to-CO reaction are written below:

1. $[CoPc] + e^- \overset{K_{[CoPc]}}{\longleftrightarrow} [CoPc]^-$
2. $[CoPc]^- + CO_2 \overset{K_{CO_2}}{\longleftrightarrow} [CO_2 - CoPc]^-$
3. $[CO_2 - CoPc]^- + H_2O \xrightarrow{k_{[CO_2-CoPc]^-}} [CO_2H - CoPc] + OH^-$
4. $[CO_2H - CoPc] \overset{K_{CO}}{\longleftrightarrow\leftrightarrow} [CO - CoPc]$

Assumption 1: Step 3 is the rate-determining step.

1. $[CoPc] + e^- \overset{K_{[CoPc]}}{\longleftrightarrow} [CoPc]^-$
2. $[CoPc]^- + CO_2 \overset{K_{CO_2}}{\longleftrightarrow} [CO_2 - CoPc]^-$
3. $[CO_2 - CoPc]^- + H_2O \xrightarrow{k_{[CO_2-CoPc]^-}} [CO_2H - CoPc] + OH^-$ RDS
4. $[CO_2H - CoPc] \overset{K_{CO}}{\longleftrightarrow\leftrightarrow} [CO - CoPc]$

The current density of CO, j_{CO}, can be represented as:

$$j_{CO} = k_{[CO_2-CoPc]^-} C([CO_2 - CoPc]^-) \quad \text{(eq. S17)}$$

Assume quasi-equilibrium for CO_2 binding, then:

$$K_{CO_2} = \frac{C([CO_2-CoPc]^-)}{C([CoPc]^-)P_{CO_2}} \quad \text{(eq. S18)}$$

Assume CO_2 as the main adsorbate, the concentration of the total active sites $[CoPc]^-_{all}$ can be represented as:

$$C([CoPc]^-_{all}) = C([CoPc]^-) + C([CO_2 - CoPc]^-) \quad \text{(eq. S19)}$$

Combine eq. S18 and eq. S19:

$$C([CO_2 - CoPc]^-) = \frac{K_{CO_2}P_{CO_2}}{1+K_{CO_2}P_{CO_2}} C([CoPc]^-_{all}) \quad \text{(eq. S20)}$$

Then we obtain the following for the current density to carbon monoxide:

$$j_{CO} = k_{[CO_2-CoPc]^-} \frac{K_{CO_2}P_{CO_2}}{1+K_{CO_2}P_{CO_2}} C([CoPc]^-_{all}) \quad \text{(eq. S21)}$$

Combining proportional terms into one parameter, k_{CO_2}**:**

$$k_{CO_2} = k_{[CO_2-CoPc]^-} C([CoPc]^-_{all}) \quad \text{(eq. S22)}$$

j_{co} can thus be written as:

$$j_{CO} = k_{CO_2} \frac{K_{CO_2}P_{CO_2}}{1+K_{CO_2}P_{CO_2}} \quad \text{(eq. S23)}$$

A good fit to the experimental results can be obtained using eq. S23, suggesting Step 3 is a likely RDS for the CO_2-to-CO reaction.

Assumption 2: Step 2 as the rate-determining step.

1. $[CoPc] + e^- \overset{K_{[CoPc]}}{\longleftrightarrow} [CoPc]^-$

2. $[CoPc]^- + CO_2 \overset{k'_{CO_2}}{\longleftrightarrow} [CO_2 - CoPc]^-$ RDS

3. $[CO_2 - CoPc]^- + H_2O \xrightarrow{K_{[CO_2-CoPc]^-}} [CO_2H - CoPc] + OH^-$

4. $[CO_2H - CoPc] \overset{K_{CO}}{\longleftrightarrow\leftrightarrow} [CO - CoPc]$

The current density of CO, j_{CO}, can be represented as:

$$j_{CO} = k'_{CO_2} C([CoPc]^-) P_{CO2} \quad \text{(eq. S24)}$$

Assume fast equilibrium for CoPc reduction, then:

$$K_{[CoPc]} = \frac{C([CoPc]^-)}{C([CoPc])\exp\left(\frac{\beta\eta F}{RT}\right)} \quad \text{(eq. S25)}$$

$$j_{CO} = k'_{CO_2} K_{[CoPc]} C([CoPc])\exp\left[\frac{\eta F}{RT}\right] P_{CO2} \quad \text{(eq. S26)}$$

Combine all constant terms into one parameter, the j_{CO} can be written as:

$$j_{CO} = k_{CO_2} P_{\mathrm{CO2}} \quad \text{(eq. S27)}$$

j_{CO} is proportional to P_{CO2} based on this hypothesis, which does not match the experimental data observed in Figure 1b. Therefore, step 2, i.e., CO_2 binding, is unlikely to be the RDS for CO_2 reduction to CO.

Numerical fitting of j_{CO}-P_{CO2} data points

We fitted the experimental j_{CO}-P_{CO2} data using eq. S21 with the MATLAB code presented in Supplementary Section 3 and the results are shown in Figure 1b. The fitted values for k_{CO_2} and K_{CO_2} are tabulated in Table S2, together with the r-square (R^2), root-mean-square deviation (RMSD) and p-value at 95% confidence interval.

Table S2. Fitted parameters for the j_{CO}-P_{CO2} data points.

k_{CO_2} (mA/cm^2)	K_{CO_2} (atm^{-1})	R^2	RMSD	p-value (95% confidence interval)	
				k_{CO_2}	K_{CO_2}
78.8	11.1	0.9693	3.52	0.000011	0.05

Supplementary Section 3: MATLAB Codes for Numerical Fitting

3.1 MATLAB code for fitting COR experimental data using eq. S12

```
% Load data
PCO = [0.02, 0.04, 0.06, 0.08, 0.1, 0.2, 0.5, 1];
jCH3OH = [0, -1.54684, -4.93146, -7.2591, -11.46504, -17.22498, -25.93561, -29.24353];

% Define parameter bounds and initial guess
lb = [0, 0];
ub = [50, 100];
x0 = [0.5, 50];

% Perform optimization
options = optimset('Display', 'iter', 'TolX', 1e-6);
```

```
params_opt = fmincon(@(params) objective_function(params, PCO, jCH3OH), x0, [], [], [], [], lb, ub, [], options);

% Extract optimized parameters
KCO_opt = params_opt(1);
KCONST_opt = params_opt(2);

% Compute model predictions using optimized parameters
PCO_model = linspace(0, 1, 1000);
j_model = KCONST_opt*KCO_opt*PCO_model./(1+KCO_opt*PCO_model);

% Plot experimental data and model predictions
figure
plot(PCO, jCH3OH, 'ro', 'MarkerSize', 10, 'LineWidth', 2)
hold on
plot(PCO_model, j_model, 'b-', 'LineWidth', 2)
xlabel('PCO')
ylabel('jMe')
legend('Experimental data', 'Model predictions')

% Output optimized parameter values
fprintf('Optimized KCO value: %f\n', KCO_opt)
fprintf('Optimized KCOSNT value: %f\n', KCO_opt)
% Calculate RMSE
RMSE = sqrt(mean((jCH3OH - KCOSNT_opt*KCO_opt*PCO./(1+KCO_opt*PCO)).^2));

% Calculate R-squared
SSresid = sum((jCH3OH - KCONST_opt*KCO_opt*PCO./(1+KCO_opt*PCO)).^2);
SStotal = (length(jCH3OH)-1) * var(jCH3OH);
```

```
R2 = 1 - SSresid/SStotal;

% Calculate p-value at 95% confidence interval
n = length(jCH3OH);
p = 2; % number of parameters
df = n - p - 1; % degrees of freedom
alpha = 0.05; % significance level
t_critical = tinv(1-alpha/2, df);
SE = sqrt(SSresid/df);
CI_lower = params_opt - t_critical*SE;
CI_upper = params_opt + t_critical*SE;
t_statistic = params_opt./SE;
p_value = 2*(1-tcdf(abs(t_statistic),df));
fprintf('RMSE: %f\n', RMSE)
fprintf('R-squared: %f\n', R2)
fprintf('90%% Confidence intervals: KCO = [%f, %f], KCONST = [%f, %f]\n', CI_lower(1), CI_upper(1), CI_lower(2), CI_upper(2))
fprintf('p-value: KCO = %f, KCONST = %f\n', p_value(1), p_value(2))
```

3.2 MATLAB code for fitting CO_2R experimental data using eq. S23

```
% Load data
PCO2 = [0.02, 0.04, 0.06, 0.08, 0.1, 0.2, 0.5, 1];
jCO = [-5.60518, -25.08095, -31.97038, -40.56943, -40.33216, -54.13102, -63.22035, -72.2163];

% Define parameter bounds and initial guess
lb = [0, 0];
ub = [100, 100];
```

```
x0 = [20, 50];

% Perform optimization
options = optimset('Display', 'iter', 'TolX', 1e-6);
params_opt = fmincon(@(params) objective_function(params, PCO2, jCO), x0, [], [], [], [], lb, ub, [], options);

% Extract optimized parameters
KCO2_opt = params_opt(1);
KCONST_opt = params_opt(2);

% Compute model predictions using optimized parameters
PCO2_model = linspace(0, 1, 1000);
j_model = KCONST_opt*KCO2_opt*PCO2_model./(1+KCO2_opt*PCO2_model);

% Calculate RMSE
RMSE = sqrt(mean((jCO - KCONST_opt*KCO2_opt*PCO2./(1+KCO2_opt*PCO2)).^2));

% Calculate R-squared
SSresid = sum((jCO - KCOSNT_opt*KCO2_opt*PCO2./(1+KCO2_opt*PCO2)).^2);
SStotal = (length(jCO)-1) * var(jCO);
R2 = 1 - SSresid/SStotal;

% Calculate p-value at 95% confidence interval
n = length(jCO);
p = 2; % number of parameters
df = n - p - 1; % degrees of freedom
alpha = 0.05; % significance level
t_critical = tinv(1-alpha/2, df);
```

```
SE = sqrt(SSresid/df);
CI_lower = params_opt - t_critical*SE;
CI_upper = params_opt + t_critical*SE;
t_statistic = params_opt./SE;
p_value = 2*(1-tcdf(abs(t_statistic),df));

% Plot experimental data and model predictions
figure
plot(PCO2, jCO, 'ro', 'MarkerSize', 10, 'LineWidth', 2)
hold on
plot(PCO2_model, j_model, 'b-', 'LineWidth', 2)
xlabel('PCO2')
ylabel('jCO')
legend('Experimental data', 'Model predictions')

% Output optimized parameter values, RMSE, R2, p-value, and confidence intervals
fprintf('Optimized KCONST value: %f\n', KCO2_opt)
fprintf('Optimized K value: %f\n', KCONST_opt)
fprintf('RMSE: %f\n', RMSE)
fprintf('R-squared: %f\n', R2)
fprintf('95%% Confidence intervals: KCO2 = [%f, %f], KCONST = [%f, %f]\n', CI_lower(1),
CI_upper(1), CI_lower(2), CI_upper(2))
fprintf('p-value: KCO2 = %f, KCONST = %f\n', p_value(1), p_value(2))
```

Supplementary Section 4: Quantum Mechanics/ Molecular Mechanics (QM/MM) Simulations

4.1 Explicit water solvation model preparation

To create the initial configurations of the explicit water solvation around the CoPc catalyst, previously reported singly reduced $[CO_2–CoPc]^-$ structures[4] were used and solvated in water using PACKMOL package[7] within a box with (15.9x15.9x15.9Å) dimensions containing 200 water molecules. The solvated structure was then optimized using Molecular Dynamics (MD) calculations as implemented within the GFN-FF xTB method.[8,9] The explicit solvated CO_2-CoPc intermediated was relaxed at 298.15K within a 15.9x15.9cx15.9Å box for 1 nanosecond with a 2 fs time step. To select the frame from the MD simulations, a structure with 4 water molecules with hydrogen bonds directed to the CO_2 adduct was chosen. To remove the excess water molecules in the explicit solvation box, using the phthalocyanine ring size, only water molecules directly on the surface of the CO_2 adsorbed CoPc side were kept, totaling 15 water molecules This MD-derived CO_2-COPc structure was then used for analysis of consecutive CO_2RR and CORR reaction steps.

4.2 QM/MM CO_2RR and CORR intermediates optimizations

All quantum chemical calculations were performed using the Q-Chem 5.2 software package.[10] Structures for the CO_2RR and CORR intermediates were modified from the explicit solvated CO_2-CoPc structure using IQmol. The B3LYP-D2 density functional[11] with 6-31G (d,p) basis sets was used for the gas-phase and explicit solvation phase Quantum Mechanics / Molecular Mechanics (QM/MM) simulations. All CoPc systems geometry optimizations were performed using a 10^{-8} strict unrestricted SCF convergence criteria and the geometry optimization tolerance gradient set to 50 x 10^{-6}. All QM/MM simulations were performed with electrostatic embedding, where Q-Chem 5.2 provided modeling of the QM region at the B3LYP-D2 level and a CHARMM27 force fields[12] describes the MM regions. Frequency calculations for CO_2RR and CORR reaction intermediates were performed using the same level of theory to correct for the Zero Point Vibrational Energy using the gas phase optimized structures. Energies in implicit solvent were determined by removing allwater molecules from the structures and by using Solvation Model Density (SMD)[13] All SMD calculations were performed using B3LYP-D2 in combination with 6-311+G**[14,15] basis on al atoms except def2-TZVP[16] on the Co atom. All reported energies correspond to QM/MM-optimized structures from which water molecules were removed for B3LYP-D2/SMD and with zero-point energy corrections.

4.3 Electrochemical potential referencing and experimental corrections

The one-electron redox potential for the CoPc/$[CoPc]^-$ couple against the Reversible Hydrogen Electrode (RHE)

$$U^{RHE} = \frac{\Delta G^o}{F} + U^{SHE} + 0.059\, x\, pH \qquad \text{(eq. S28)}$$

where F is the Faraday constant, ΔG^o is the Gibbs Free Energy difference between the $[CoPc]^-$ and CoPc species, and U^{SHE} is the reference potential for the Standard Hydrogen Electrode (SHE) valued at 4.44 V.[17] The pH was set to 8.5 to contrast with the set experimental data. For the solvation free energy of a proton $\Delta G_{solv}(H^+)$, a value of −265.9 kcal/mol.[18]

The free energy profiles calculated for each reaction intermediates correspond to the following reaction steps:

CO_2 Reduction Reaction (CO_2RR) Mechanism:

(1) $CoPc\ (I) + e^- \rightarrow [CoPc]^-\ (II)$ (Step I→II)

(2) $[CoPc]^-\ (II) + CO_2 \rightarrow [CO_2-CoPc]^-(III)$ (Step II→III)

(3) $[CO_2-CoPc]^-(III) + H^+ \rightarrow [CO_2H-CoPc]\ (IV)$ (Step III→IV)

(4) $[CO_2H-CoPc]\ (IV) + H^+ + e^- \rightarrow [CO-CoPc]\ (VI) + H_2O$ (Step IV→VI)

(5) $[CO-CoPc]\ (VI) \rightarrow CoPc(I) + CO$ (Step VI→I)

(6) $[CO-CoPc]\ (VI) + e^- \rightarrow [CO-CoPc]^-(VII)$ (Step VI→VII)

(7) $[CO-CoPc]^-(VII) \rightarrow [CoPc]^-(II) + CO$ (Step VII→II)

CO Reduction Reaction (CORR) Mechanism:

(1) $CoPc\ (I) + e^- \rightarrow [CoPc]^-(II)$ (Step I→II)

(2) $[CoPc]^-(II) + CO \rightarrow [CO-CoPc]^-(VII)$ (Step II→VII)

(3) $[CO-CoPc]^-\ (VII) + H^+ \rightarrow [HCO-CoPc]\ (VIII)$ (Step VII→VIII)

(4) $[HCO-CoPc]\ (VIII) + H^+ + e^- \rightarrow [HCOH-CoPc]\ (IX)$ (Step VIII→IX)

(5) $[HCOH-CoPc]\ (IX) + H^+ + e^- \rightarrow [H_2COH-CoPc]\ (X)$ (Step IX→X)

(6) $[H_2COH-CoPc]^-\ (X) + H^+ + e^- \rightarrow [H_3COH-CoPc]\ (XI)$ (Step X→XI)

(7) $[H_3COH-CoPc]\ (XI) \rightarrow CH_3OH + CoPc\ (I)$ (Step XI→I)

(8) $[H_3COH-CoPc]\ (XI) + e^- \rightarrow [H_3COH-CoPc]^-(II)$ (Step XI→II)

(9) $[H_3COH\text{–}CoPc]^{-}(XI) \rightarrow CH_3OH + [CoPc]^{-}(II)$ (Step XI→II)

4.4 Gibbs free energy analysis for CO_2 and CO equilibrium constant on the singly reduced CoPc catalyst

Considering the Gibbs free energy for the binding of CO_2 and CO molecules to the singly reduced CoPc catalyst, the ratio of the equilibrium constants ($\frac{K_{CO_2}}{K_{CO}}$) was computed as:

$$\frac{K_{CO_2}}{K_{CO}} = e^{\frac{[\Delta G_{CO} - \Delta G_{CO_2}]}{k_B T}} \quad \text{(eq. S29)}$$

Here k_B is the Boltzmann constant ($1.99\text{x}10^{-3}\ \frac{kcal}{mol\ K}$) , ΔG is the Gibbs free energy for CO_2 and CO binding the singly reduced CoPc catalyst and T is the temperature (298.15 K).

Table S3. Energies for all CO_2RR optimized CoPc structures used for calculating each elementary step Gibbs Free Energy (ΔG). All energies are reported in kcal/mol.

Species	**$E+G_{solv}$**	**ZPVE**	**H_{vib}**	**Temperature (K)**	**S_{vib}**
CoPc	-1914244.552	260.617	276.044	298.150	0.096
$[CoPc]^-$	-1914351.901	260.617	276.044	298.150	0.096
$[CO_2\text{-}CoPc]^-$	-2224695.592	332.311	356.378	298.150	0.156
$[CO_2H\text{-}CoPc]$	-2081002.584	292.651	311.776	298.150	0.122
[CO-CoPc]	-2033388.014	280.195	299.695	298.150	0.128
$[CO\text{-}CoPc]^-$	-2033464.041	278.596	298.378	298.150	0.133
CO_2	-118375.483	7.281	7.46	298.150	0.001
CO	-2033388.014	280.195	299.695	298.150	0.128
H_2O	-47987.031	13.399	13.401	298.150	0.000
H_2	-738.567	6.387	6.387	298.150	0.000

Supplementary Section 5: Supplementary Figures

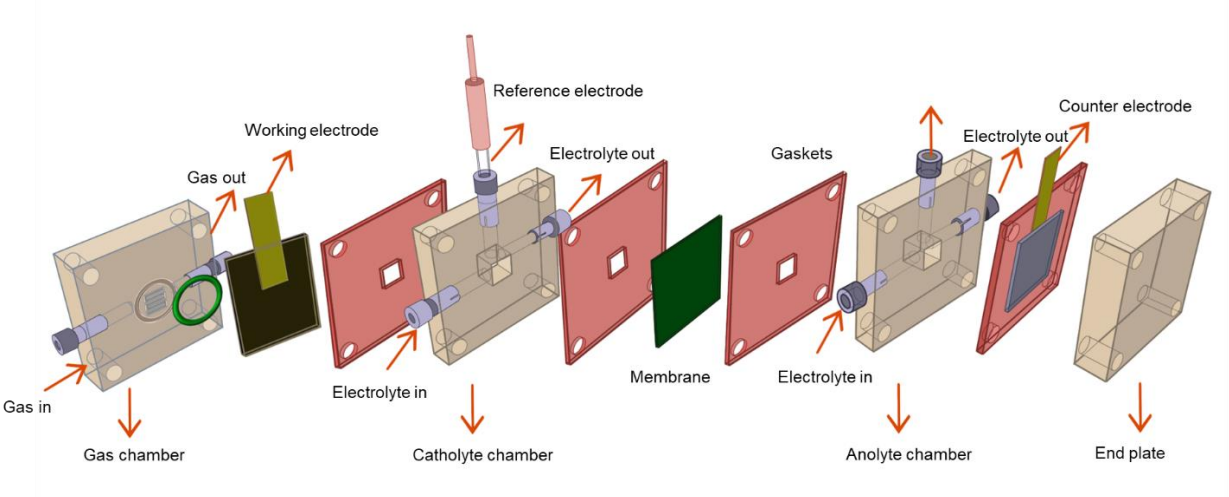

Figure S1. Exploded view of the flow cell assembly.

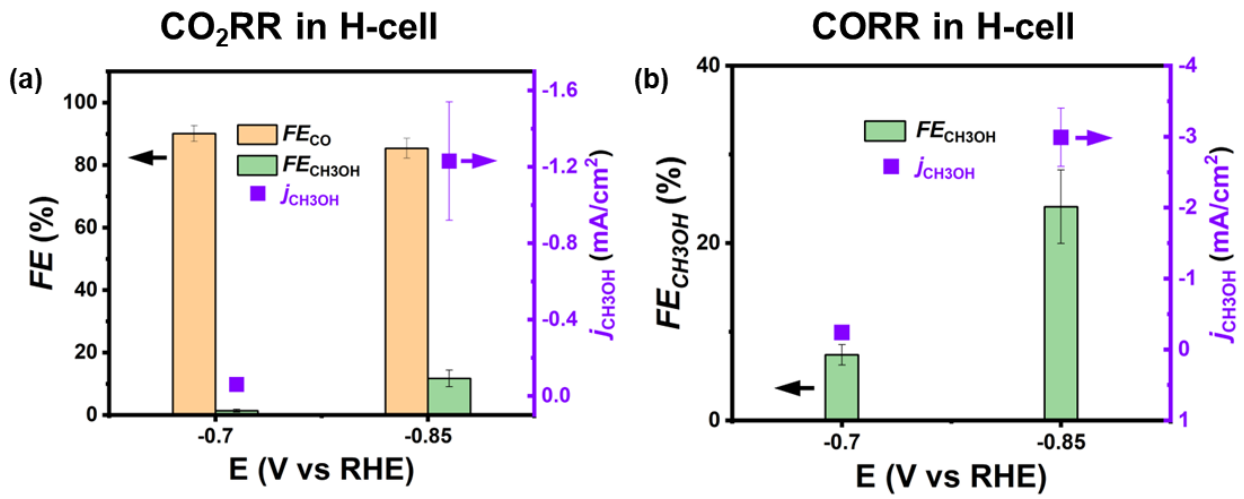

Figure S2. (a) CO_2RR and (b) CORR performance by CoPc/MWCNT in aqueous H-cell. All reactions were carried out in 0. 5 M $KHCO_3$ electrolyte with adjusted pH of 8.5.

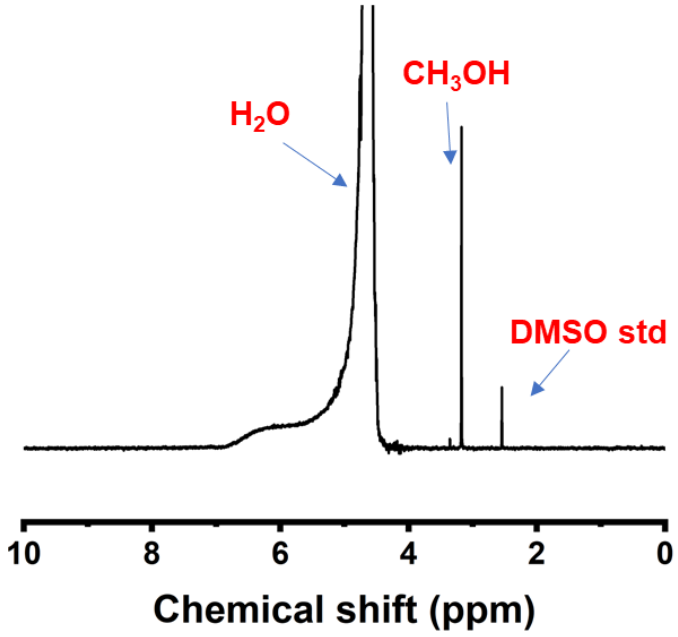

Figure S3. Demonstration of a typical ^{1}H NMR spectrum for the liquid product after CO/CO_2 electrolysis. Methanol is the only detectable liquid product, in addition to the DMSO standard internally added to the sample. The liquid sample shown is obtained from CO reduction using 1 atm CO gas under −0.7 V (RHE). The electrolyte used is 0.5 M $KHCO_3$ with pH=8.5.

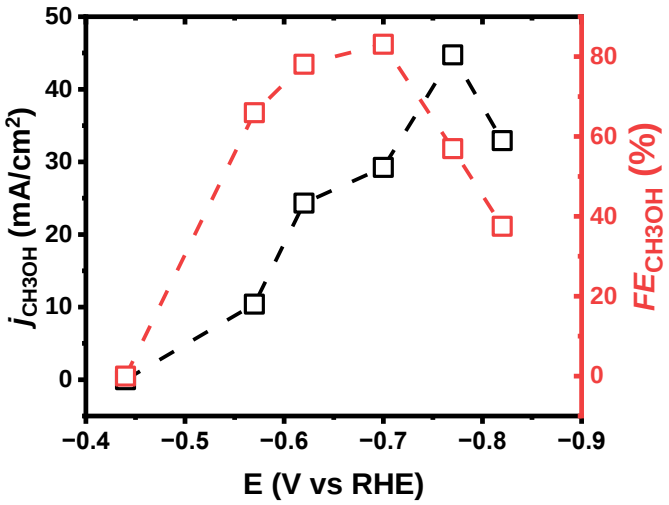

Figure S4. Potential-dependent j_{CH3OH} (mA/cm^2) and FE_{CH3OH} (%) for CO reduction on CoPc GDE. All reactions were conducted with 1 atm CO gas under −0.7 V (RHE) with 0.5 M $KHCO_3$ electrolyte (pH=8.5).

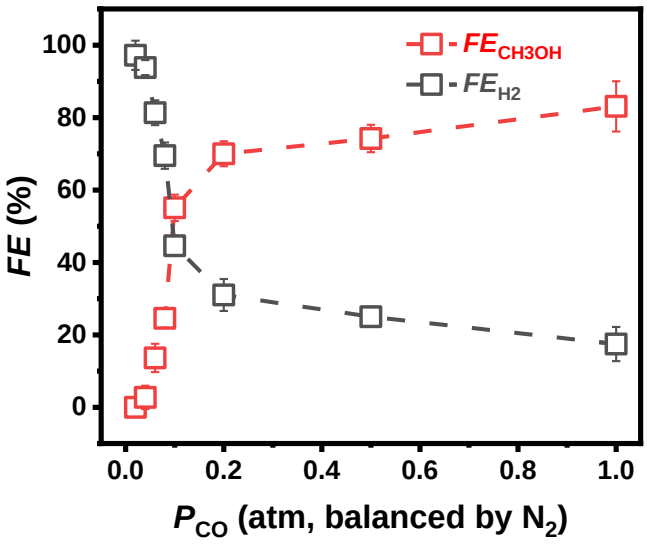

Figure S5. P_{CO}-dependent FE_{CH3OH} (%) for CO reduction on CoPc GDE. All reactions were carried out at −0.7 V (RHE) with 0.5 M $KHCO_3$ electrolyte (pH=8.5).

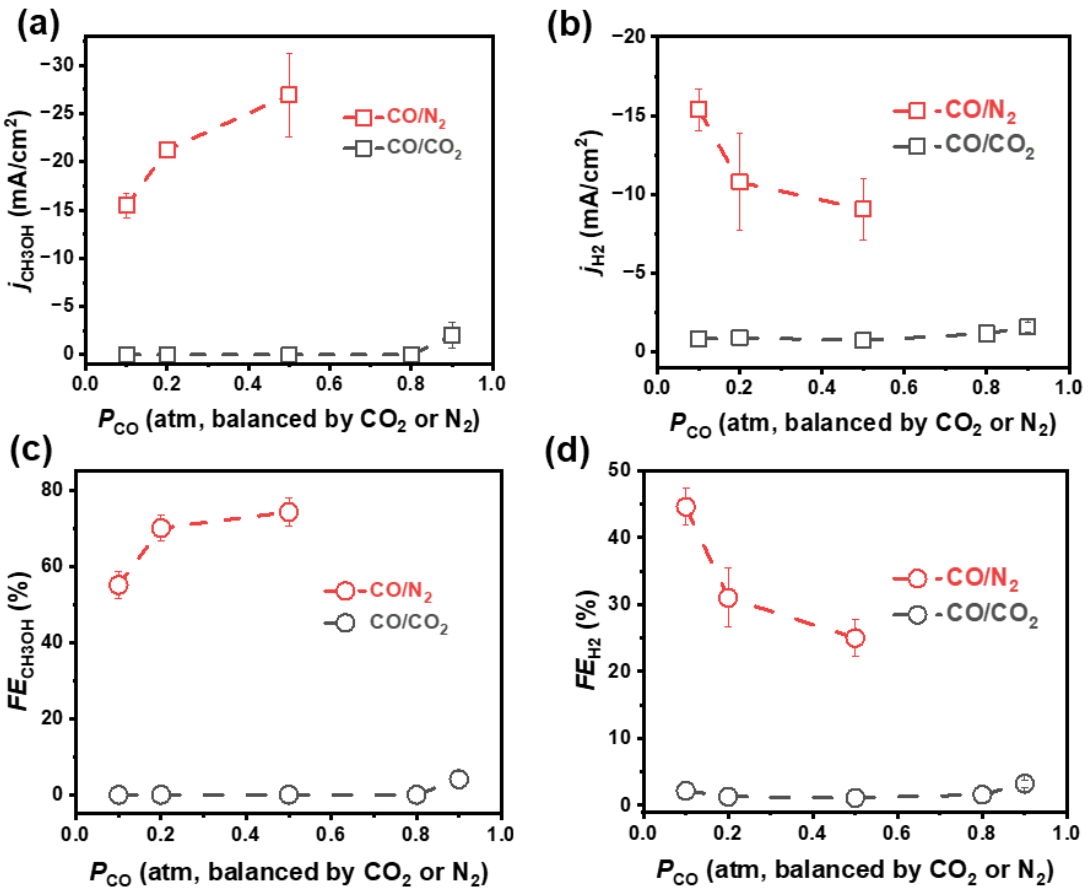

Figure S6. Comparison of methanol and H_2 production performance between CO/CO_2 and CO/N_2 gas mixtures. (a) j_{CH3OH}. (b) j_{H2}. (c) FE_{CH3OH}. (d) FE_{H2}. The performance between 0.90 and 0.98 atm P_{CO} is compared and presented in Figure 2a and b. All reactions were carried out at −0.7 V (RHE) with 0.5 M $KHCO_3$ electrolyte (pH=8.5). The total gas flow rate is controlled at 15 mL/min.

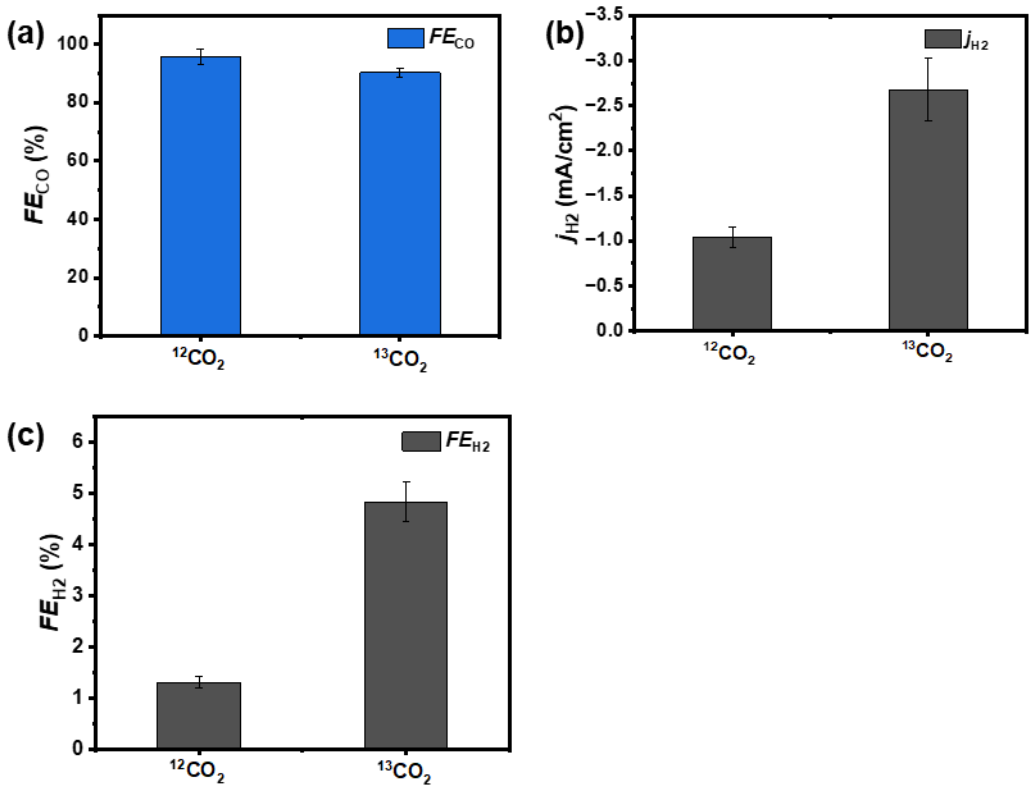

Figure S7. Comparison of CO_2RR performance between ^{12}C and ^{13}C isotopologues. (a) FE_{CO}. (b) j_{H2}. (c) FE_{H2}. All reactions were carried out with 1 atm CO_2 gases at −0.7 V (RHE) with 0.5 M $KHCO_3$ electrolyte (pH=8.5).

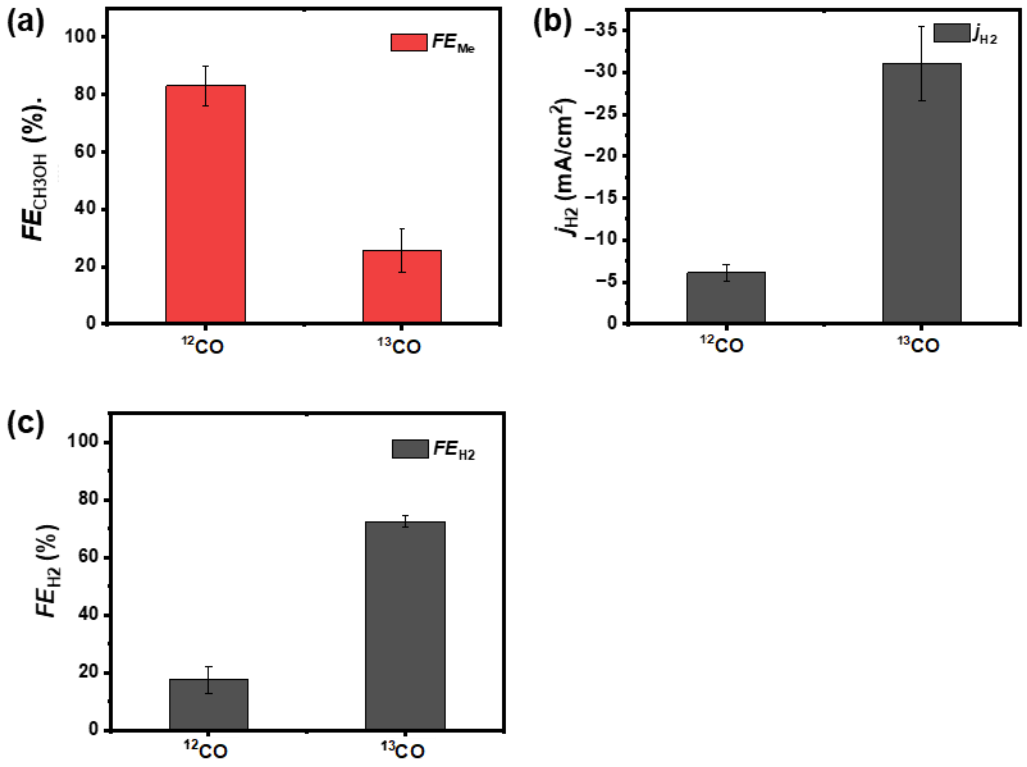

Figure S8. Comparison of CORR performance between ^{12}C and ^{13}C isotopologues. (a) FE_{CH3OH}. (b) j_{H2}. (c) FE_{H2}. All reactions were carried out with 1 atm CO gases at −0.7 V (RHE) with 0.5 M $KHCO_3$ electrolyte (pH=8.5).

References

(1) Yao, L.; Yin, C.; Rivera-Cruz, K. E.; McCrory, C. C. L.; Singh, N. Translating Catalyst–Polymer Composites from Liquid to Gas-Fed CO_2 Electrolysis: A CoPc-P4VP Case Study. *ACS Appl. Mater. Interfaces* **2023**, acsami.3c04085. https://doi.org/10.1021/acsami.3c04085.

(2) Chang, X.; Li, J.; Xiong, H.; Zhang, H.; Xu, Y.; Xiao, H.; Lu, Q.; Xu, B. C−C Coupling Is Unlikely to Be the Rate-Determining Step in the Formation of C2+ Products in the Copper-Catalyzed Electrochemical Reduction of CO. *Angew. Chem.* **2022**, *134* (2), e202111167. https://doi.org/10.1002/ange.202111167.

(3) Zhu, M.; Ye, R.; Jin, K.; Lazouski, N.; Manthiram, K. Elucidating the Reactivity and Mechanism of CO_2 Electroreduction at Highly Dispersed Cobalt Phthalocyanine. *ACS Energy Lett.* **2018**, *3* (6), 1381–1386. https://doi.org/10.1021/acsenergylett.8b00519.

(4) Rivera Cruz, K. E.; Liu, Y.; Soucy, T. L.; Zimmerman, P. M.; McCrory, C. C. L. Increasing the CO_2 Reduction Activity of Cobalt Phthalocyanine by Modulating the σ-Donor Strength of Axially Coordinating Ligands. *ACS Catal.* **2021**, *11* (21), 13203–13216. https://doi.org/10.1021/acscatal.1c02379.

(5) Liu, Y.; McCrory, C. C. L. Modulating the Mechanism of Electrocatalytic CO2 Reduction by Cobalt Phthalocyanine through Polymer Coordination and Encapsulation. *Nat. Commun.* **2019**, *10* (1), 1683. https://doi.org/10.1038/s41467-019-09626-8.

(6) Li, J.; Chang, X.; Zhang, H.; Malkani, A. S.; Cheng, M.; Xu, B.; Lu, Q. Electrokinetic and in Situ Spectroscopic Investigations of CO Electrochemical Reduction on Copper. *Nat. Commun.* **2021**, *12* (1), 3264. https://doi.org/10.1038/s41467-021-23582-2.

(7) Martínez, L.; Andrade, R.; Birgin, E. G.; Martínez, J. M. PACKMOL: A package for building initial configurations for molecular dynamics simulations. *J. Comput. Chem.* **2009**, *30* (13), 2157–2164. https://doi.org/10.1002/jcc.21224.

(8) Grimme, S.; Bannwarth, C.; Shushkov, P. A Robust and Accurate Tight-Binding Quantum Chemical Method for Structures, Vibrational Frequencies, and Noncovalent Interactions of Large Molecular Systems Parametrized for All Spd-Block Elements (Z= 1–86). *J. Chem. Theory Comput.* **2017**, *13* (5), 1989–2009.

(9) Spicher, S.; Grimme, S. Robust Atomistic Modeling of Materials, Organometallic, and Biochemical Systems. *Angew. Chem. Int. Ed.* **2020**, *59* (36), 15665–15673.

(10) Shao, Y.; Gan, Z.; Epifanovsky, E.; Gilbert, A. T.; Wormit, M.; Kussmann, J.; Lange, A. W.; Behn, A.; Deng, J.; Feng, X. Advances in Molecular Quantum Chemistry Contained in the Q-Chem 4 Program Package. *Mol. Phys.* **2015**, *113* (2), 184–215.

(11) Grimme, S. Semiempirical GGA-type Density Functional Constructed with a Long-range Dispersion Correction. *J. Comput. Chem.* **2006**, *27* (15), 1787–1799.

(12) MacKerell Jr, A. D.; Banavali, N.; Foloppe, N. Development and Current Status of the CHARMM Force Field for Nucleic Acids. *Biopolym. Orig. Res. Biomol.* **2000**, *56* (4), 257–265.

(13) Marenich, A. V.; Olson, R. M.; Kelly, C. P.; Cramer, C. J.; Truhlar, D. G. Self-Consistent Reaction Field Model for Aqueous and Nonaqueous Solutions Based on Accurate Polarized Partial Charges. *J. Chem. Theory Comput.* **2007**, *3* (6), 2011–2033.

(14) Clark, T.; Chandrasekhar, J.; Spitznagel, G. W.; Schleyer, P. V. R. Efficient Diffuse Function-augmented Basis Sets for Anion Calculations. III. The 3-21+ G Basis Set for First-row Elements, Li–F. *J. Comput. Chem.* **1983**, *4* (3), 294–301.

(15) Krishnan, R.; Binkley, J. S.; Seeger, R.; Pople, J. A. Self-consistent Molecular Orbital Methods. XX. A Basis Set for Correlated Wave Functions. *J. Chem. Phys.* **1980**, *72* (1), 650–654.
(16) Weigend, F.; Ahlrichs, R. Balanced Basis Sets of Split Valence, Triple Zeta Valence and Quadruple Zeta Valence Quality for H to Rn: Design and Assessment of Accuracy. *Phys. Chem. Chem. Phys.* **2005**, *7* (18), 3297–3305.
(17) Trasatti, S. The Absolute Electrode Potential: An Explanatory Note (Recommendations 1986). *Pure Appl. Chem.* **1986**, *58* (7), 955–966. https://doi.org/10.1351/pac198658070955.
(18) Tissandier, M. D.; Cowen, K. A.; Feng, W. Y.; Gundlach, E.; Cohen, M. H.; Earhart, A. D.; Coe, J. V.; Tuttle, T. R. The Proton's Absolute Aqueous Enthalpy and Gibbs Free Energy of Solvation from Cluster-Ion Solvation Data. *J. Phys. Chem. A* **1998**, *102* (40), 7787–7794.